A Finite Element Study of Stable Crack Growth Under Plane Stress Conditions: Part II—Influence of Hardening

R. Narasimhan
Research Fellow in Applied Mechanics.

A. J. Rosakis
Assistant Professor of Aeronautics and Applied Mechanics. Assoc. Mem. ASME

J. F. Hall
Assistant Professor of Civil Engineering.

Division of Engineering and Applied Science, California Institute of Technology, Pasadena, CA 91125

A detailed finite element analysis is performed to model quasi-static crack growth under plane stress, small-scale yielding conditions in elastic-plastic materials characterized by isotropic power law hardening and the Huber-Von Mises yield surface. A nodal release procedure is used to simulate crack extension. Results pertaining to the influence of hardening on the extent of active yielding and the near-tip stress and deformation fields are presented. Clear evidence of an elastic unloading wake following the active plastic zone is found, but no secondary (plastic) reloading along the crack flank is numerically observed for any level of hardening. A ductile crack growth criterion based on the attainment of a critical crack opening displacement at a small microstructural distance behind the tip, is employed to investigate the nature of the J resistance curves under plane stress. In addition, the same criterion is employed to investigate the influence of hardening on the potential for stable crack growth under plane stress. It is found that predictions based on a perfectly plastic model may be unconservative in this respect, which is qualitatively similar to the conclusions reached in antiplane shear and Mode I plane strain.

1 Introduction

Several investigators have contributed in providing an understanding of the mechanics of stable crack growth by using both analytical and numerical techniques. Such works are reviewed in the introduction of Part I of the present investigation.

In this part a detailed finite element analysis is undertaken to model crack growth under plane stress in isotropic power hardening solids. This is a continuation of our earlier work (Narasimhan and Rosakis, 1986), which analyzed the monotonic loading of a stationary crack. Two crack growth histories (see Section 2) are simulated to study the mechanics problem of quasi-static crack extension and also to investigate the initial phase of stable growth under small-scale yielding, as would be observed in an experiment.

2 Numerical Analysis

Formulation. The numerical modeling of the Mode I plane stress, small-scale yielding problem was discussed in detail by Narasimhan and Rosakis (1986), who performed the analysis of a monontically loaded stationary crack. In the present investigation, the results obtained by them will be used as initial conditions to simulate quasi-static crack extension. The basic features of the numerical analysis have been summarized in Part I.

Constitutive Assumptions. The material model that was considered here was that of an elastic-plastic solid with an isotropic power law hardening behavior. A small strain incremental plasticity theory was employed along with the Huber-Von Mises yield condition and the associated flow rule. The Huber-Von Mises yield condition for isotropic hardending takes the form,

$$f(\sigma,\bar{\epsilon}^p) = F(\sigma) - \bar{\sigma}^2(\bar{\epsilon}^p), \tag{2.1}$$

where $F(\sigma) = 3/2\ \mathbf{S}\cdot\mathbf{S}$, and $\bar{\epsilon}^p = \int(2/3\epsilon^p_{ij}\epsilon^p_{ij})^{1/2}dt$ is the accumulated equivalent plastic strain. In the above, $\mathbf{S}$ is the deviatoric stress tensor, and $\bar{\sigma}(\bar{\epsilon}^p)$ is defined by the following power hardening rule,

$$\frac{\bar{\epsilon}^p}{\epsilon_0} = \left(\frac{\bar{\sigma}}{\sigma_0}\right)^n - \frac{\bar{\sigma}}{\sigma_0}. \tag{2.2}$$

Here σ_0 and ϵ_0 are the yield stress and strain in uniaxial tension.

The total strain rate tensor is assumed to be decomposed into elastic and plastic parts, and the constitutive law for material currently experiencing plastic deformation is given by,

Contributed by the Applied Mechanics Division for presentation at the Winter Annual Meeting, Boston, MA, December 13–18, 1987, of the American Society of Mechanical Engineers.

Discussion on this paper should be addressed to the Editorial Department, ASME, United Engineering Center, 345 East 47th Street, New York, N.Y. 10017, and will be accepted until two months after final publication of the paper itself in the JOURNAL OF APPLIED MECHANICS. Manuscript received by ASME Applied Mechanics Division, December 10, 1986; final revision May 21, 1987.
Paper No. 87-WA/APM-21.

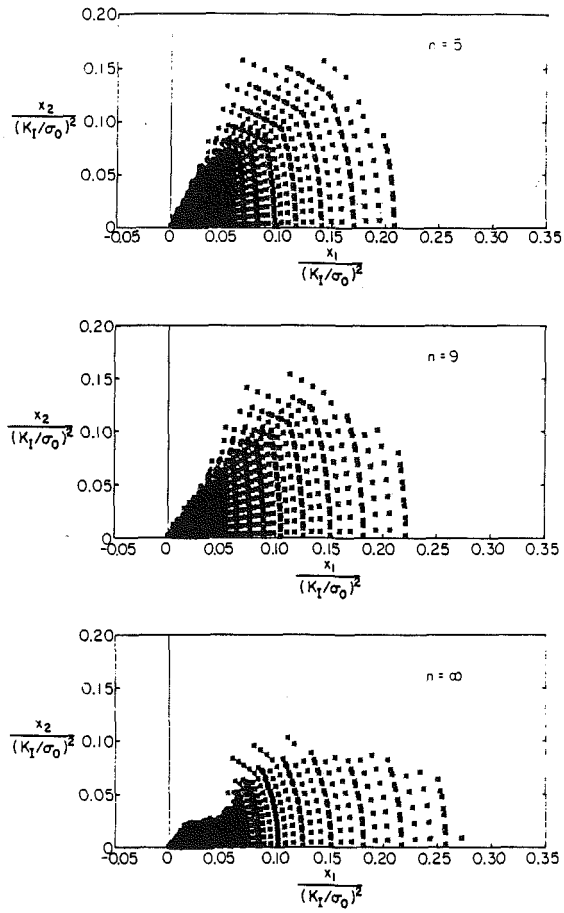

Fig. 1 Active plastic zone surrounding the propagating crack tip for various levels of hardening

$$\dot{\sigma}_{ij} = C^*_{ijkl}\dot{\epsilon}_{kl}$$

$$= \left[C_{ijkl} - \frac{C_{ijpq}S_{pq}S_{mn}C_{mnkl}}{S_{rt}C_{rtuv}S_{uv} + \frac{4}{9}\bar{\sigma}^2 H} \right] \dot{\epsilon}_{kl}. \tag{2.3}$$

Here C_{ijkl} is the isotropic, positive definite elasticity tensor and $H = d\bar{\sigma}/d\bar{\epsilon}^p$, which can be obtained from (2.2). In the present analysis, the yield criterion and the constitutive law were used along with the plane stress condition,

$$\sigma_{3i} \equiv 0. \tag{2.4}$$

On using equation (2.4) in (2.3), a constraint for $\dot{\epsilon}_{33}$ in terms of $\dot{\epsilon}_{\alpha\beta}$ may be obtained.

The computations were performed for two levels of hardening, $n = 5$ and 9. The ratio of the Young's modulus to the yield stress in pure shear (E/τ_0) was taken as 1400 and the Poisson's-ratio as 0.3 in the calculations.

Solution Strategy. In this study, two simple crack growth histories were simulated employing the nodal release procedure (see Part I and also Narasimhan et al. 1986). In the first case, the maximum plastic zone extent at the end of the stationary loading process was slightly more than 50 times the smallest element size L. Subsequently, twenty one-element crack growth steps were simulated using the nodal release procedure, holding the externally applied load fixed. This was achieved by imposing $T \equiv (E/\sigma_0^2)dJ/da = 0$ during crack growth. T is the nondimensional Paris tearing modules. The purpose of this investigation is to examine the nature of the near-tip stress and deformation fields for the mechanics problem of quasi-static crack growth without the influence of increase in applied load. Following Rice (1975), this would correspond to a hypothetical situation in which a cracked specimen is initially loaded by clamping portions of its boundary and imposing displacements, which is then followed by crack extension by saw-cutting ahead under fixed boundary displacements.

However, in an actual situation, after initiation, a crack will generally grow stably in an elastic-plastic material for an extent typically of the order of a few plastic zone sizes, during which the applied load will have to be increased to propagate the crack. A steady-state condition will then be reached, after which no further increase in applied load will be required for additional crack growth. In the second load history, stable crack extension was modelled (in a continuous manner) by simultaneously increasing the applied load during the nodal release procedure. This was accomplished by simulating fifteen one-element crack growth steps under $T = 1.5$, following the stationary loading process. The maximum extent of the plastic zone was over 100 times the smallest element length, L. Only the material with $n = 9$ was considered in this investigation.

In the following section, detailed results will be presented initially for $n = 5$ and 9 corresponding to the first load history. At the end of the section, comparison between the results for the two load histories will be made for the material with $n = 9$.

3 Results and Discussion

Active Plastic Zones. The active plastic zone surrounding the propagating crack tip after the twentieth crack growth step is shown in Fig. 1 for $n = 5$ and 9, in moving coordinates that have been made dimensionless by the self-similar parameter $(K_I/\sigma_0)^2$. The plastic zone for the stable plane stress crack growth in an elastic-perfectly plastic material is also shown for comparison.[1] The current crack tip is at the origin of the coordinate system, and a point in the figure represents an actively yielding integration station within an element.

A large elastic unloading region can be seen following the active plastic zone. No secondary (plastic) reloading along the crack flank has been observed for any level of hardening from the present numerical solution. The asymptotic angular extent of the active plastic zone, θ_p, decreases with decreasing hardening (increasing n). The values of θ_p are approximately 65 deg, 55 deg, and 45 deg for $n = 5$, 9, and ∞, respectively. The maximum radial extent of the active plastic zone, R_p, which occurs directly ahead of the crack tip, increases with decreasing hardening. The values of R_p are about $0.22(K_I/\sigma_0)^2$, $0.24(K_I/\sigma_0)^2$, and $0.28(K_I/\sigma_0)^2$ for $n = 5$, 9, and ∞, respectively.

Comparison of Fig. 1 with the plastic zone surrounding the stationary crack (Narasimhan and Rosakis, 1986) show that the active plastic zone becomes more acute (sharper) with the onset of crack growth. The results for the stationary problem show rounded plastic zones for the hardening cases, with yielding spreading beyond 90 deg near the crack tip. Strong changes in the near-tip plastic zone shape occurred during the first few crack growth steps, and then the overall features were unaltered with subsequent crack advance. The maximum radial extent of the plastic zone, R_p, given above for the propagation crack, is about the same as in the stationary problem for all levels of hardening.

A kink in the trailing boundary of the active plastic zone (Fig. 1) appears to develop for materials with low hardening and it becomes pronounced for the perfectly plastic case. The reason for this development could be related to the change in

[1] Throughout this paper, results given as $n = \infty$ will correspond to the perfectly plastic crack growth analysis of Part I.

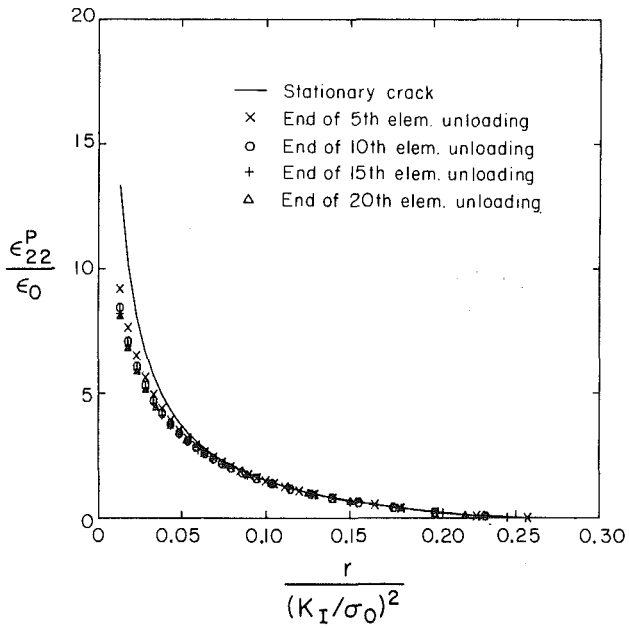

Fig. 2 Radial distribution of plastic strain ahead of the propagating crack tip for various levels of crack growth under fixed applied load for a material with $n = 9$

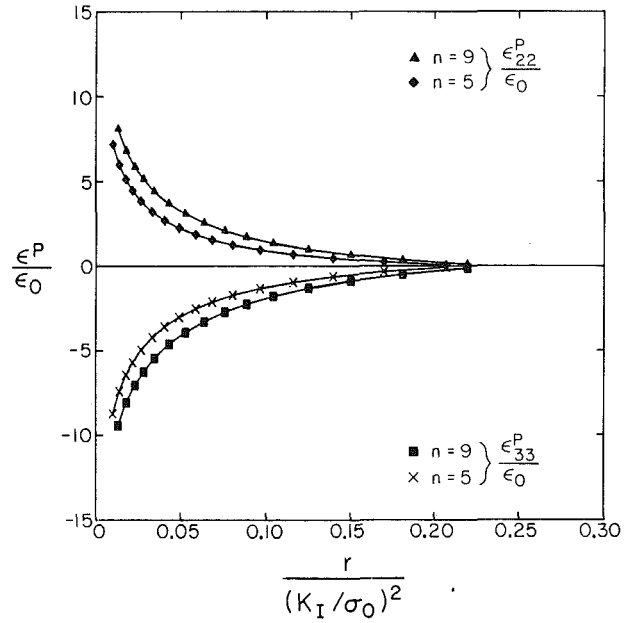

Fig. 3 Radial distribution of plastic strain ahead of the propagating crack tip at the end of the twentieth crack growth step at fixed applied load for $n = 5$ and 9

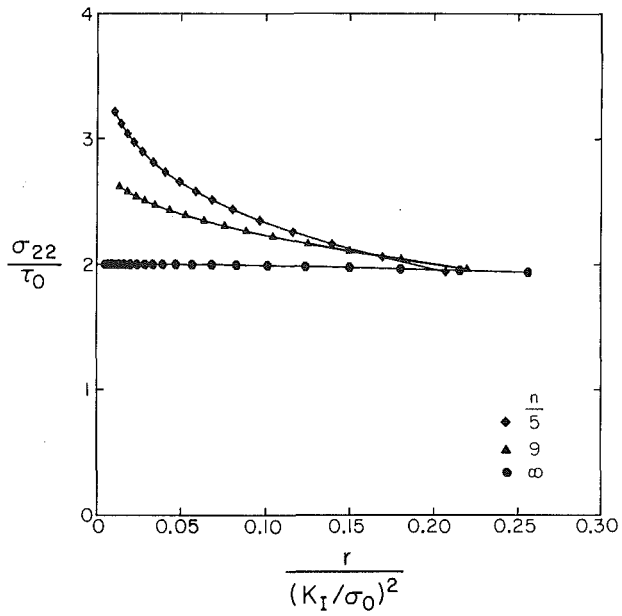

Fig. 4 Radial distribution of opening stress ahead of the moving tip

nature of the governing equations (from elliptic to hyperbolic), in the limit as the perfectly plastic case is approached. Such a behavior can also be observed from the plastic zone shapes given by Dean and Hutchinson (1980) for crack growth under antiplane shear in a linear hardening material. The similarity between the present plane stress plastic zone shapes and their antiplane shear results stems from the presence of an intense deformation zone ahead of the crack tip in both cases.

The active plastic zones of Fig. 1 and the corresponding results obtained by Dean (1983) for steady-state crack growth under plane stress in a linear hardening material have essentially the same features. However, one difference seems to be the absence of the kink in the active plastic zone for the perfectly plastic limit in Dean's solution. Nevertheless, the present analysis is more detailed, because it has a larger ratio of plastic zone to smallest element size as compared with that of Dean's computation. Also, unlike his work, the initial phase of crack growth was modelled in the present investigation.

Radial Distribution of Plastic Strains. The radial distribution of the normalized plastic strain, $\epsilon^p_{22}/\epsilon_0$, with respect to normalized distance, $r/(K_I/\sigma_0)^2$, ahead of the propagating crack tip is shown in Fig. 2 for a material with $n = 9$. Results are presented for various levels of crack growth at fixed applied load, along with the plastic strain distribution ahead of a monotonically loaded stationary crack tip, which was obtained by Narasimhan and Rosakis (1986). As can be seen from this figure, the plastic strain ahead of the moving crack tip converges rapidly during the first few crack growth steps to an invariant distribution. For example, at a distance of $r = 0.013$ $(K_I/\sigma_0)^2$ ahead of the moving tip, the plastic strain dropped by 30 percent during the first five crack growth steps and by 8 percent, 3 percent, and 1.5 percent during the sixth to tenth steps, eleventh to fifteenth steps, and sixteenth to twentieth steps, respectively.

Such rapid convergence was typical of the other hardening case ($n = 5$) as well as the perfectly plastic material. The weaker singularity in the plastic strains near the tip during crack growth, as compared with the stationary problem in Fig. 2, is due to the fact that the crack propagates into material that has already deformed plastically (Rice, 1975). The radial distribution of the plastic strains ahead of the tip at the end of the twentieth release step is shown in Fig. 3 for the two levels of hardening, $n = 5$ and 9.

Radial Distribution of Stresses. The radial distribution of the normalized opening stress, σ_{22}/τ_0, ahead of the moving crack tip is shown in Fig. 4 for $n = 5$ and 9, along with the perfect plasticity solution. As can be seen from this figure, the stress components become more strongly singular with increasing hardening. The perfect plasticity solution for σ_{22} tends to a bounded value of $1.999\tau_0$, as the crack tip is approached along the $\theta = 0$ ray, and is in excellent agreement with the preliminary asymptotic result of Rice (1982). This asymptotic limit was the same as that obtained by the numerical solution near the stationary crack tip.

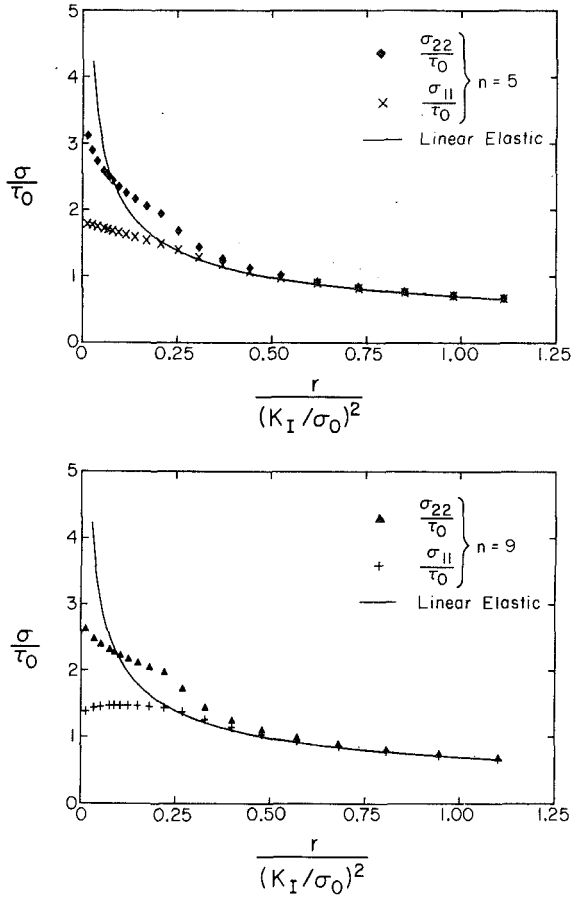

Fig. 5 Comparison of radial stress distribution ahead of the moving tip as given by the K_I field (solid line) with the finite element solution for (*a*) $n = 5$ and (*b*) $n = 9$

The stress variation for the hardening materials in Fig. 4 also differs only slightly from the stationary crack distribution, for moderate to large distances from the tip. For example, at a distance of $r = 0.018\ (K_I/\sigma_0)^2$ ahead of the tip, the ratio of the opening stress for the propagating crack to that for the stationary problem is 3.04/3.13 and 2.58/2.66 for $n = 5$ and 9, respectively. Also, as pointed out by Narasimhan and Rosakis (1986), the stress distribution (Fig. 4) appears to be relatively insensitive to the hardening level for distances from the tip exceeding about $0.15\ (K_I/\sigma_0)^2$.

In order to study the influence of the crack tip plastic zone on the stress field in the surrounding elastic region, the radial stress distribution ahead of the moving crack tip is shown on an expanded scale for $n = 5$ and 9 in Fig. 5. The singular elastic solution (K_I field) is also indicated by the solid line in the figure, for comparison. The distribution of stresses outside the plastic zone is almost identical to the corresponding result obtained for the stationary problem. The σ_{22} stress component obtained from the numerical solution differs strongly (by more than 30 percent) from that given by the K_I field at the elastic-plastic boundary ($r = R_p$). But a rapid transition in the stress distribution takes place immediately outside the plastic zone and the stresses agree closely with those of the K_I field for $r > 1.5\ R_p$.

Near-Tip Angular Distribution of Stresses. The near-tip angular distribution of the normalized polar stress components is shown in Fig. 6 for $n = 5$ and 9 along with the perfect plasticity solution. The centroidal values of stresses in the elements lying on a rectangular contour surrounding the moving crack tip, with an average radius of $0.018\ (K_I/\sigma_0)^2$ (which is within $0.08\ R_p$), have been used to make this plot. The angular variation along the above contour of the Von Mises equivalent stress, $\sigma_{eqv} = (3/2 s_{ij} s_{ij})^{1/2}$, which has been made dimensionless by σ_0, is also shown in the figure.

The assertion made earlier, that no secondary (plastic) reloading was observed (as $\theta \rightarrow 180$ deg) for any level of

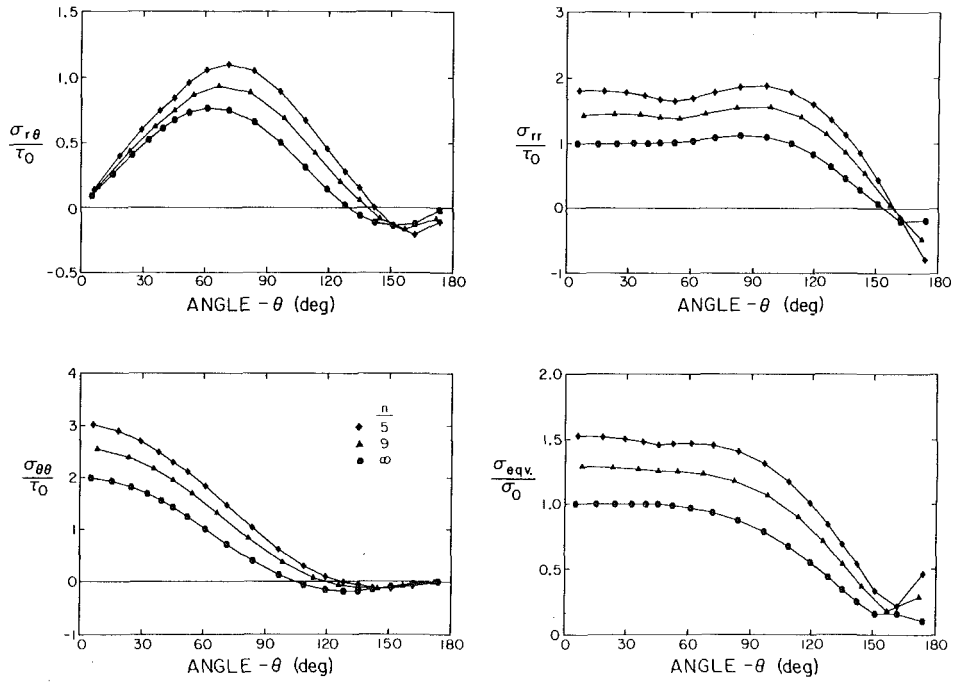

Fig. 6 Near-tip angular distribution of the normalized polar stress components and the Von Mises equivalent stress at a distance of $0.018\ (K_I/\sigma_0)^2$ from the moving tip

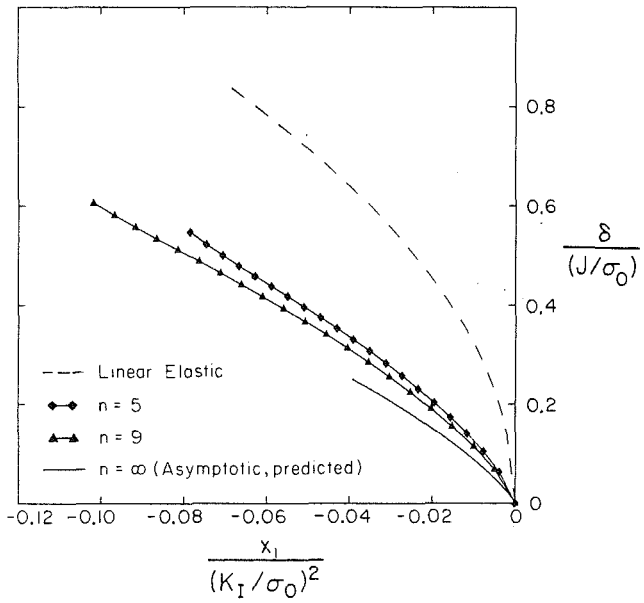

Fig. 7 Numerically obtained crack opening profiles for quasi-static crack growth under fixed applied load for n = 5 and 9. The dashed line is th linear elastic asymptotic solution and the solid line is the asymptotic crack displacement for steady-state crack growth in a perfectly plastic solid, as predicted in Part I.

hardening, is confirmed from this figure. Also, elastic unloading occurs for angles θ greater than about 65 deg, 55 deg, and 45 deg for n = 5, 9, and ∞, respectively, although it is not obvious from this figure for the hardening cases. The near-tip angular stress variation for the hardening materials appears to be qualitatively similar to the perfectly plastic case. As noted in Part I, the angular stress variation within the active plastic zone for the perfectly plastic case is in very good agreement with the distribution in a centered fan, as predicted by Rice (1982).

Crack Opening Profiles. The normalized crack opening displacement, $\delta/(J/\sigma_0)$, versus normalized distance, $x_1/(K_I/\sigma_0)^2$, along the crack flank is shown in Fig. 7 for the two hardening cases, n = 5 and 9, when the crack grows under fixed applied load. This profile was obtained after twenty crack growth steps and was self-similar in normalized form, in the sense that it was almost identical for different levels of crack growth. The crack opening profile for a linear elastic material is also shown by the dashed line in the figure.

The steady-state asymptotic opening profile for a crack growing in a perfectly plastic material, as predicted in Part I, is indicated by a solid line in the figure. This is given by,

$$\frac{\delta}{(J/\sigma_0)}=\beta\eta ln\left(\frac{es}{\eta}\right), \tag{3.1}$$

where

$$\eta=r/(K_I/\sigma_0)^2.$$

In the above equation e is the base of the natural logarithm. The parameters β and s which occur in equation (3.1) were estimated in Part I as 1.70 and 0.60, respectively, from a best-fit to the near-tip crack displacement increment, obtained from the numerical solution for the nonhardening case.

It can be noticed from Fig. 7 that the crack profiles vary considerably with the hardening level. This was also observed by Dean (1983) from his steady-state solution for plane stress crack growth in linear hardening solids. This also appears to be true for the crack profiles obtained under antiplane shear by Dean and Hutchinson (1980). However, the crack profiles under Mode I plane strain show comparatively less variation with the hardening level, at least near the crack tip (e.g., Dean and Hutchinson, 1980). Also, as opposed to the blunted shapes obtained for the stationary problem, the crack opening profiles during growth (Fig. 7) are sharp. This is directly traceable to the permanence of plastic deformation (Rice, 1975).

4 Ductile Crack Growth Criterion

Perfect Plasticity. Rice and Sorensen (1978) and Rice et al. (1980) proposed that a critical opening displacement, $\delta = \delta_C$, should be maintained at a small microstructural distance, r_c, behind the crack tip for continued crack growth. The near-tip crack displacement during continuous stable crack extension (see Section 3, Part I) can be written as

$$\delta=\beta\left(\frac{\sigma_0}{E}\right)rln\left(\frac{\rho}{r}\right), \quad r\to 0, \tag{4.1}$$

where

$$\rho=Re^{(1+T\alpha/\beta)}. \tag{4.2}$$

In the above equation, $R = sEJ/\sigma_0^2$ for small-scale yielding and T is the tearing modulus. The parameters α, β, and s, which occur in equation (4.2), were estimated in Part I as 0.82, 1.70, and 0.60 respectively. The crack growth criterion stated above requires that the parameter ρ, which uniquely characterizes the near-tip crack profile, be constant for continued crack extension.

Thus, on estimating ρ from J_C and T_0, which are the values of the far-field J and the tearing modulus T at the onset of crack growth, it is possible to obtain the following differential equation for J as function of crack length a (Rice et al., 1980),

$$T=\frac{E}{\sigma_0^2}\frac{dJ(a)}{da}=T_0-\frac{\beta}{\alpha}ln\left(\frac{J}{J_C}\right). \tag{4.3}$$

By using $J = J_C$ and $a = a_0$ as initial conditions the above equation can be integrated to give,

$$\frac{a-a_0}{(EJ_C/\sigma_0^2)}=\frac{\alpha}{\beta}e^{(\alpha T_0/\beta)}\left[E_i\left\{-\frac{\alpha T_0}{\beta}\right\}-E_i\left\{ln\left(\frac{J}{J_C}\right)-\frac{\alpha T_0}{\beta}\right\}\right], \tag{4.4}$$

where $E_i\{\cdot\}$ is the exponential integral function. It is interesting to note that the mathematical structure of equations (4.3) to (4.4) are similar to the ones deduced by Wnuk (1974) by means of his "final stretch" crack growth criterion, based on a plane-stress Dugdale, line plastic zone model.

A family of plane stress resistance curves generated from equation (4.4) corresponding to several values of T_0 with α and β taken as 0.82 and 1.70, respectively, is shown in Fig. 8. The abscissa of the figure is the extent of crack growth, made dimensionless by the quantity $0.3EJ_C/\sigma_0^2$, which is approximately equal to the maximum plastic zone extent at initiation. The flat portion of the curves corresponds to steady state crack growth when no further increase in externally applied J is required to propagate the crack. Setting $dJ/da = 0$ in (4.3) gives J corresponding to steady-state as

$$J_{SS}=J_Ce^{\alpha T_0/\beta}. \tag{4.5}$$

Comparison of Fig. 8 with the corresponding plot for plane strain given by Rice et al. (1980) show that the amount of stable crack extension in plane stress if far more extensive than in plane strain. This is because the ratio α/β in plane stress as computed in the present investigation, is 0.82/1.70, which is about 4.4 times larger than the corresponding ratio of 0.6/5.46 in plane strain (Rice, 1982; Sham, 1983). Thus, for T_0 = 5, the ratio J_{SS}/J_C calculated from (4.5) is 11.2 and 1.73 for plane stress and plane strain, respectively.

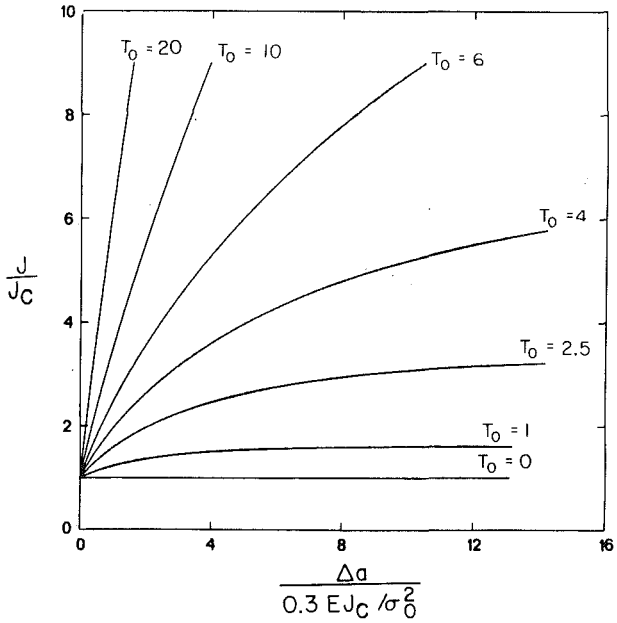

Fig. 8 Predicted normalized plane stress J resistance curves. The abscissa is the amount of crack growth normalized by a quantity which is approximately equal to the maximum plastic zone extent at initiation.

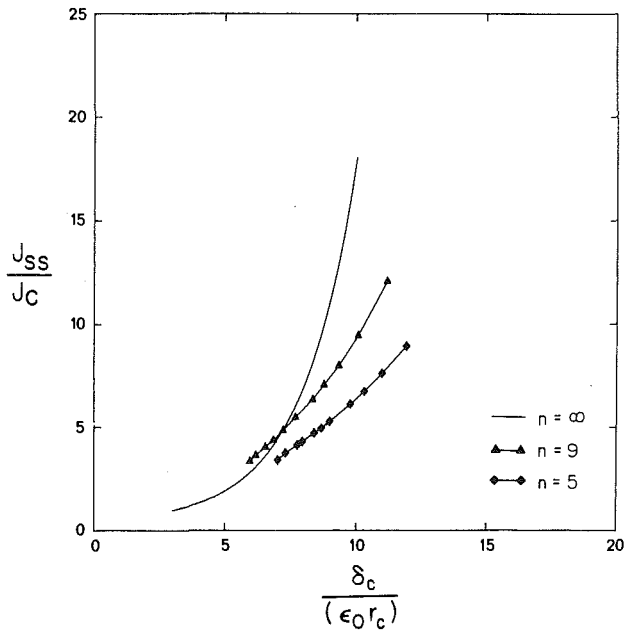

Fig. 10 Influence of hardening on J_{SS}/J_C in Mode I plane stress, as predicted by the critical displacement criterion, for continued crack growth. The solid line is the perfect plasticity result of Part I.

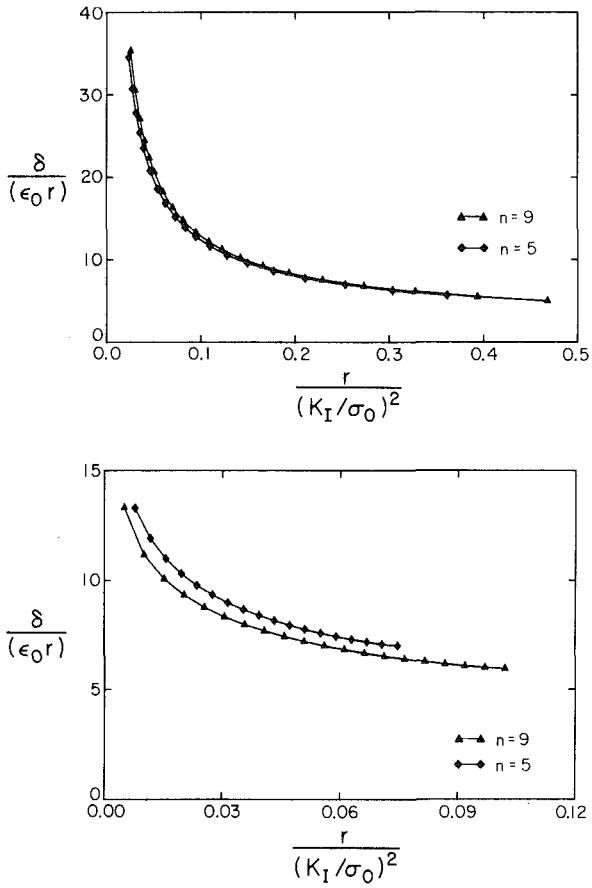

Fig. 9 Variation of $\delta/(\epsilon_0 r)$ with normalized distance along the crack flank for (*a*) the stationary problem (Narasimhan and Rosakis, 1986) and (*b*) quasi-static crack growth under fixed applied load

Hardening Solid. The above crack growth criterion can be used for both initiation and continuation at crack growth (Dean and Hutchinson, 1980) to examine the potential for stable growth from the microstructural viewpoint. To this end, the crack proflies shown in Fig. 7 for crack growth under fixed applied load were taken as steady-state profiles and were used to generate a plot of $\delta/(\epsilon_0 r)$ versus $r/(K_{SS}/\sigma_0)^2$. This is shown in Fig. 9(*b*) for the two cases of hardening, $n = 5$ and 9. The opening displacement for the stationary crack given by Narasimhan and Rosakis (1986) was used similarly to obtain the variation of $\delta/(\epsilon_0 r)$ versus $r/(K_C/\sigma_0)^2$ as shown in Fig. 9(*a*).

For a given value of the microscale parameter $\lambda_m = \delta_C/(\epsilon_0 r_c)$, the value of $r_c/(K_{SS}/\sigma_0)^2$ can be obtained from the abscissa of Fig. 9(*b*) corresponding to steady-state crack growth. The value of $r_c/(K_{IC}/\sigma_0)^2$ may be obtained similarly from Fig. 9(*a*) for initiation of crack growth. These two quantities can be used to compute the ratio of $J_{SS}/J_C = (K_{SS}/K_C)^2$, corresponding to the chosen value of the microscale parameter λ_m. The variation of J_{SS}/J_C versus $\delta_C/(\epsilon_0 r_c)$, calculated as indicated above for $n = 5$ and 9, is shown in Fig. 10. On comparing Figs. 9(*a*) and 9(*b*), it can be seen that the influence of hardening on the relationship between J_{SS}/J_C and $\delta_C/(\epsilon_0 r_c)$ arises mainly due to the results in Fig. 9(*b*), corresponding to steady-state crack growth. The effect of hardening on the variation of $\delta/(\epsilon_0 r)$ with respect to $r/(K_C/\sigma_0)^2$ at initiation is not so significant, as can be seen from Fig. 9(*a*).

For comparison purposes, the variation of J_{SS}/J_C with respect to $\delta_C/(\epsilon_0 r_c)$ for the elastic-perfectly plastic material, is also shown in Fig. 10 by the solid line. It can be shown from equations (4.1)–(4.3), along with the fact that $\delta_C = \alpha J_C/\sigma_0$ for initiation, that this relation is given by,

$$\frac{J_{SS}}{J_C} = \frac{\alpha}{s\lambda_m} e^{(\lambda_m/\beta - 1)}, \tag{4.6}$$

where $\lambda_m = \delta_C/(\epsilon_0 r_c)$. It can be seen from Fig. 10 that in the range $\mu_m > 8.0$, the ratio J_{SS}/J_C may increase significantly with a decrease in hardening. For example, corresponding to a value of $\lambda_m = 9.5$, the ratio J_{SS}/J_C is 5.8, 8.3, and 14.1 for $n = 5$, 9, and ∞, respectively. Thus, the potential for stable crack growth may be grossly overestimated by a calculation based on the perfect plasticity idealization, when the material actually possesses some hardening. Hence, predictions about the extent of stable crack growth based on the perfectly plastic

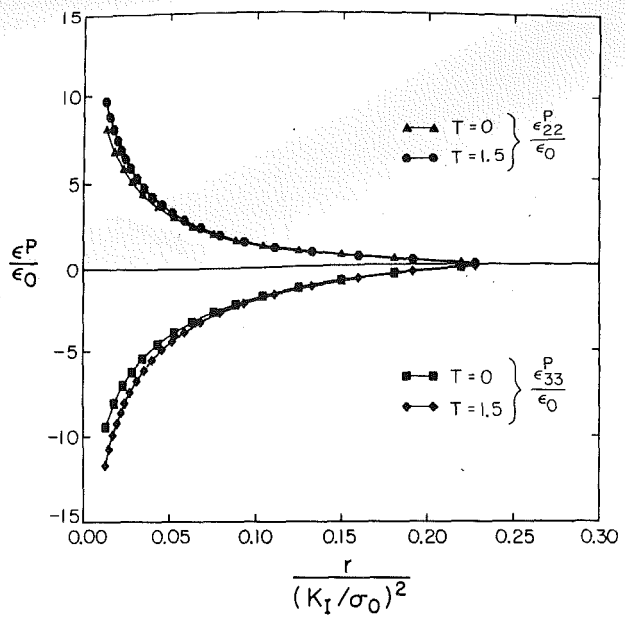

Fig. 11 Comparison of the radial distribution of plastic strains ahead of the tip for the two crack growth histories that were simulated for n = 9

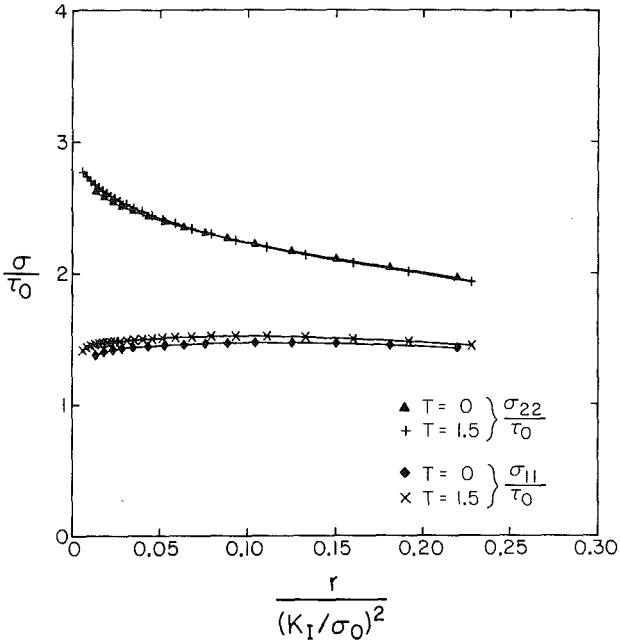

Fig. 12 Radial stress distribution ahead of the tip for n = 9 for the two crack growth histories

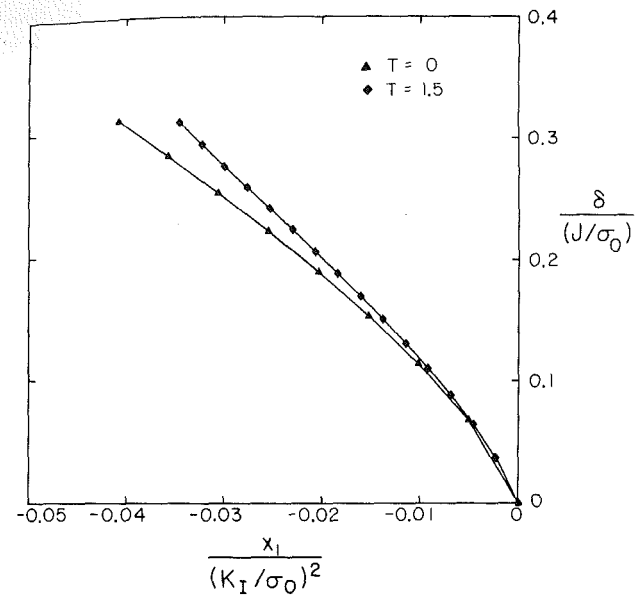

Fig. 13 Effect of increase in applied load at T = 1.5 on the near-tip crack displacement for n = 9

model may be unconservative for a hardening material when the microscale parameter exceeds a value of about 8. A qualitatively similar conclusion was reached in antiplane shear and Mode I plane strain as well, by Dean and Hutchinson (1980).

In the light of the above observation, one is compelled to examine the effects of kinematic hardening and corner formation on the yield surface, which may occur during the nonproportional loading experienced by a material particle near the crack tip. It is not clear to what extent these factors will affect the potential for stable crack growth under plane stress conditions. Dean and Hutchinson (1980) found that the influence of corner formation was not as significant as strain hardening from their numerical results for antiplane shear crack growth. However, Lam and McMeeking (1984) observed that both corner formation and kinematic hardening further reduced the potential for stable crack growth in Mode I plane strain. Thus, in this sense, even the results based on a smooth yield surface with isotropic hardening may be unconservative. It is suggested that such effects should be investigated in Mode I plane stress.

5 Comparison of Results for the Two Crack Growth Histories

In order to study the influence of increase in applied load, as would be observed in an experiment during the initial phase of stable crack extension, a crack growth history at a constant value of T = 1.5 was also simulated in this work. Only the material with n = 9 was considered in this investigation.

The active plastic zones obtained for this crack growth history compared very closely with that shown in Fig. 1, both in shape and size. During the first few crack growth steps, the active plastic zone assumed the sharpened shape of Fig. 1, which did not change with subsequent crack advance. The values of θ_p and R_p were about 55 deg and 0.24 $(K_I/\sigma_0)^2$ as reported earlier, based on the first crack growth history (at fixed applied load).

The plastic strains ahead of the moving crack tip exhibited a tendency to converge rapidly to an invariant distribution during the first few crack growth steps as in the earlier analysis (Fig. 2). The normalized plastic strains ahead of the tip at the end of the fifteenth crack growth step under T = 1.5 is shown in Fig. 11 and is compared with the result given in Fig. 3 for crack growth at T = 0. As expected, the plastic strains for T = 1.5 are slightly higher due to the influence of increase in applied load with crack growth.

The radial distribution of stresses ahead of the propagating crack tip for the two histories is shown in Fig. 12 in the nondimensional form, $\sigma_{\alpha\beta}/\tau_0$ versus $r/(K_I/\sigma_0)^2$. The effect of the increase in applied load on the stress field seems to be less significant than that on the deformation field. Also, the near-tip angular stress distribution for the two histories were almost identical. Finally, the nondimensional crack opening displacement, $\delta/(J/\sigma_0)$, as a function of position on the crack flank, $x_1/(K_I/\sigma_0)^2$, is shown in Fig. 13 for T = 0 and 1.5. Due to the increase in applied load, the crack opening displacement for T = 1.5 is higher than that for T = 0.

Acknowledgment

The authors would like to express their gratitude to Professor J. W. Knowles for his valuable advice and encouragement. This investigation was supported by the Office of Naval Research through ONR contract #N00014-85-K-0596. The computations were performed using the Supercomputer at Boeing Computer Services, Seattle. This was made possible through NSF contract #MEA-8307785. The above contracts and the facilities provided by Boeing Computer Services are gratefully acknowledged.

References

Dean, R. H., 1983, "Elastic-Plastic Steady Crack Growth in Plane Stress," *Elastic-Plastic Fracture: Second Symposium, Volume I-Inelastic Crack Analysis*, ASTM STP 803, pp. I-39–I-51.

Dean, R. H., and Hutchinson, J. W., 1980, "Quasi-Static Steady Crack Growth in Small-Scale Yielding," *Fracture Mechanics: Twelfth Conference*, ASTM STP 700, pp. 385–400.

Lam, P. S. and McMeeking, R. M., 1984, "Analysis of Steady Quasistatic Crack Growth in Plane Strain Tension in Elastic-Plastic Materials with Non-Isotropic Hardening," *Journal of Mechanics and Physics of Solids*, Vol. 32, pp. 395–414.

Narasimhan, R., and Rosakis, A. J., 1986, "A Finite Element Analysis of Small-Scale Yielding near a Stationary Crack under Plane Stress," Caltech Report SM 86-21, Pasadena, CA, *Journal of Mechanics and Physics of Solids*, to appear, 1988.

Narasimhan, R., Rosakis, A. J., and Hall, J. F., 1986, "A Finite Element Study of Stable Crack Growth under Plane Stress Conditions in Elastic-Perfectly Plastic Solids," Caltech Report SM 86-22, Pasadena, CA.

Rice, J. R., 1975, "Elastic-Plastic Models for Stable Crack Growth," *Mechanics and Mechanisms of Crack Growth*, May, N. J., ed., British Steel Corp. Physical Metallurgy Centre Publication, Sheffield, England, pp. 14–39.

Rice, J. R., 1982, "Elastic-Plastic Crack Growth," *Mechanics of Solids*, Hopkins, H. G., and Sewell, M. J., eds., Pergamon Press, Oxford, pp. 539–562.

Rice, J. R., and Sorensen, E. P., 1978, "Continuing Crack-Tip Deformation and Fracture for Plane Strain Crack Growth in Elastic-Plastic Solids," *Journal of Mechanics and Physics of Solids*, Vol. 26, pp. 163–186.

Rice, J. R., Drugan, W. J., and Sham, T. L., 1980, "Elastic-Plastic Analysis of Growing Cracks," *Fracture Mechanics: Twelfth Conference*, ASTM STP 700, pp. 189–221.

Sham, T. L., 1983, "A Finite Element Study of the Asymptotic Near-Tip Fields for Mode I Plane Strain Cracks Growing Stably in Elastic-Ideally Plastic Solids," *Elastic-Plastic Fracture: Second Symposium, Volume I—Inelastic Crack Analysis*, ASTM STP 803, pp. 52–79.

Wnuk, M. P., 1974, "Quasi-static Extension of a Tensile Crack Contained in a Viscoelastic-Plastic Solid," ASME JOURNAL OF APPLIED MECHANICS, Transactions of ASME, Ser. E, Vol. 41, pp. 231–242.